Appl Nanosci (2016) 6:1043–1052
DOI 10.1007/s13204-016-0519-x

ORIGINAL ARTICLE

Lithium–germanium–phosphate glassceramic electrolytes: correlation between the nanocrystallization and electrical studies

Ch. Krishna Kishore Reddy[1] · G. Suman[1] · R. Balaji Rao[1] · Naresh Kumar Katari[2] · M. R. P. Reddy[3]

Received: 9 November 2015 / Accepted: 11 January 2016 / Published online: 29 January 2016

Abstract Investigations on the microstructural and electrical properties of a glassceramic system: $(100 - x)[0.4Li_2O - 0.1GeO_2 - 0.6P_2O_5] + x$ [20 h ball milled Ga_2O_3] ($0 \leq x \leq 10$ mol%, in the regular steps of 2 mol%) via high-energy ball milling technique are reported. XRD spectra of LGePG glassceramic samples were identified major crystalline phases such as $Li_3Ge_2(PO_4)_3$ (NASICON-type phase), $Ga_2Li_3(PO_3)_7$ and GeO_2 from the major diffraction peaks. Bulk conductivity of all these samples was measured for the powder-compressed pellets by ac impedance method. The correlation of $\log(\sigma)$ and M'' peaks suggests the presence of single conduction mechanism in the LGePG glassceramic samples. The results are discussed in the light of degree of crystallization of lithium phosphate glass network.

Keywords Glasses · X-ray diffraction · Electrical properties

Introduction

Recently, solid-state glassceramic electrolytes when precipitated with superionic nanocrystals, they got attracted because of their remarkable electrical conductivity (Al-Hartomy et al. 2013; Fanelli et al. 2011; El-Desoky 2010). Among the oxide and sulfide-based glassceramic electrolytes, the ionic conductivity of sulfide-based compounds is superior over oxide based counter parts. However, sulfides are not chemically stable over longer durations than oxides (Kim et al. 2008, Kim and Jeong 2011). Oxide-based glassceramic electrolytes are highly preferred because they posses excellent chemical and mechanical stability even under heavy loads, nevertheless, their ionic conductivity barely meets the required power densities of the cell (Kim et al. 2008, Kim and Jeong 2011; Hayashi et al. 2012). On the other hand, NASICON-based glassceramic type structure was given top priority as it facilitates the fast diffusion pathways for monovalent ions which is the necessary and sufficient condition for boosting the conductivity at least by two orders (He et al. 2014).

Though, several routes were taking place to enhance ionic conductivity amorphous electrolyte materials, precipitation of nanocrystals in the glass and glassceramic materials via high-energy ball milling was regarded as highly efficient choice, where nanoscaled powders of electrodes directly mixed with electrolytes, leads to reduce the interfacial resistance and also surface modification under room temperature and normal pressure (Kang et al. 2003; Xu and Gao 2004; Lam et al. 2004; Dell et al. 2007; Reddy et al. 2012). Furthermore, it is also to be noted down that the uniform distribution of fine grains of nanocrystalline phases in the glass and glassceramic structure can significantly produce fast diffusion path ways and hence, desirable ionic conductivity is expected to achieve (Dell et al. 2007; Reddy et al. 2012). Ga_2O_3 is a good chemically and thermally stable material whose quantum size effects will influence largely on Li–Ge–P network for its high Li ion conductivity, thermal stability, and physical properties (Prasad et al. 2005). On the other

✉ R. Balaji Rao
ravuri3091@yahoo.co.in

[1] Department of Physics, GITAM University, Hyderabad Campus, Hyderabad, India

[2] Department of Chemistry, GITAM University, Hyderabad Campus, Hyderabad, India

[3] Center for Materials for Electronics Technology, Hyderabad, India

hand, the role of GeO_2 in this glassceramic matrix significantly improves the phase immiscibility during its transition from glass to the glassceramic matrix which is a fundamental property to control the degree of crystallization. In view of this, correlation between the mechanism of crystallization and its electrical transport is worthwhile to discuss for the use in the high-energy density applications (Prasad et al. 2005).

We have already reported in our investigation that the estimated mean sizes for the 20 h ball milled Ga_2O_3 nanocrystallites are obtained by using the Scherrer's formula for half width of the diffraction peaks of the all the in the lithium titatanate phosphate glass ceramic samples vary in between 12 and 17 nm along with little larger clusters ~20–50 nm in size for the 20 h ball mill which was chosen for dispersion in L–Ge–P glassceramic matrix. However, beyond 20 h the powder gets strained (Reddy et al. 2012).

Experimental

The glassceramic samples with general formulae: $(100 - x)$ $[0.4Li_2O - 0.1GeO_2 - 0.6P_2O_5] + x$ [20 h ball milled Ga_2O_3]; $(0 \leq x \leq 10$ mol%, in the steps of 2 mol%) have been synthesized by high-energy ball milling technique, labeled as $LGePG_x$ (where x is the mol% of 40 h ball milled Ga_2O_3) from the mixtures of analytical reagent-grade chemicals of Li_2CO_3, P_2O_5, GeO_2 and Ga_2O_3. Glassceramic samples are prepared by heating the mechanically milled glasses over their crystallization temperatures. The synthesis procedure to conceive final powders and their green pellets is as published from our laboratory (Reddy et al. 2012). Green pellets thus obtained were sintered over their crystalline temperatures at 2 °C/min and then cooled down to room temperature in the furnace without any plateau stage. The DTA traces were recorded in the temperature range of 300–1300 K using analytical grade Al_2O_3 as a reference material by using DT-30 Schimadzu thermal analyzer (error ±2 K) in flowing nitrogen by heating at 20 K/min. The degree of crystallization of phases was studied by XRD method using PANanalytical Diffractometer B.V fitted with Cu target (both $K\alpha_1 + \alpha_2$ wavelengths) and Ni filter at 40 kV and 30 mA (2θ range). The electrical conductivity studies were carried out using a computer-controlled Solatron 1260 Impedance/Gain phase analyzer with pellet specimens of 10 mm diameter and about 3 mm thick. The silver coating was applied on both sides of pellet. Measurements were made conducted in the frequency range of $10–10^6$ Hz at room temperature and as well as temperatures from 303 to 423 K with a 10 K temperature step in dry Ar atmosphere.

Results and discussion

DTA patterns obtained for all the LGePG glassceramic samples are shown in the Fig. 1. It is to be noted that crystallization phenomenon can be treated as an exothermic process in glasses and glassceramic materials in view of the fact that the free energy of crystalline phase is lower than that of glassy phase. The exothermic peak related to the crystallization temperatures T_c (tangent at the inflexion point) for the possible crystalline phases varies from 877 to 841 K. Where as endothermic related to glass transition T_g (intercept of the base line) changes from 802 to 751 K from the sample $LGePG_0$ to $LGePG_6$, however, from $LGePG_8$ to $LGePG_{10}$, the trend is reversed. The glass transition temperature (T_g) decreases from $LGePG_0$ to $LGePG_6$ which shows their increasing trend of de-polymerization. However, increasing trend in the lattice strain is indicated by the increase in the glass transition temperature (T_g) from the $LGePG_6$ (751 K) to $LGePG_{10}$ (791 K). Nevertheless, the glass stability parameter (K_{gl}) is a good estimate of the glass forming tendency; higher is K_{gl} value, more stable is the glass and less critical is the quenching rate. It can be calculated from the DTA parameters using the relation

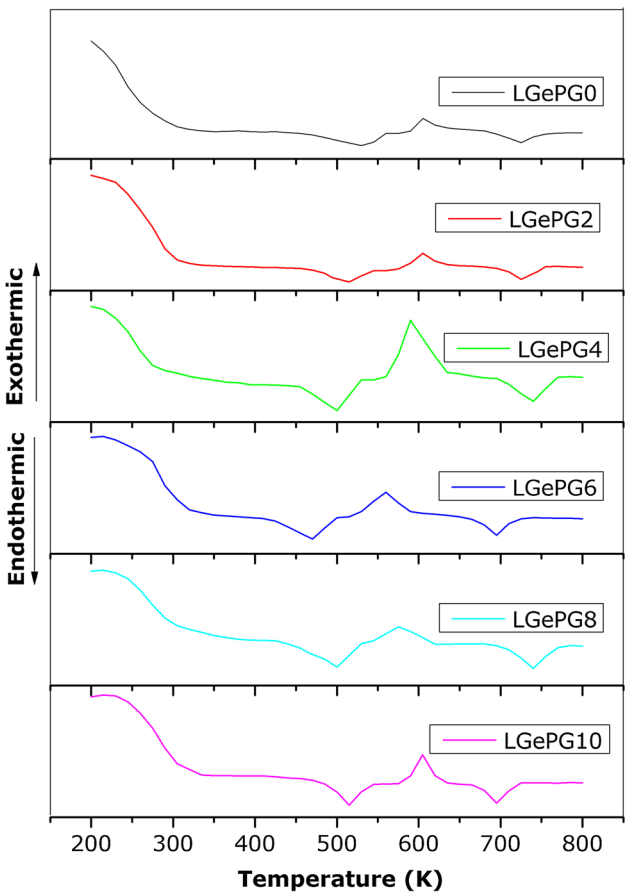

Fig. 1 DTA traces of for all the LGePG glassceramic samples

Table 1 Summary of DTA data for all the samples of LGePG glassceramic samples

Sample	T_g (K)	ΔT ($T_c - T_g$ (K)	$K_{gl} = (T_c - T_g)/(T_m - T_c)$
$LGePG_0$	620	40	0.620
$LGePG_2$	612	36	0.609
$LGePG_4$	601	33	0.592
$LGePG_6$	**583**	**28**	**0.579**
$LGePG_8$	592	30	0.598
$LGePG_{10}$	608	35	0.611

The best result is set in bold

($K_{gl} = (T_c - T_g)/(T_m - T_c)$) and it should be noted down that for good glass forming systems, the value of K_{gl} should be greater than or equal to unity (Hruby 1972). The details of DTA parameters for all the LGePG samples are listed in Table 1. The decreasing trend in the value of K_{gl} from $LGePG_0$ (0.620) to $LGePG_6$ (0.579), denotes the decrease in the degree of de-polymerization, however, from $LGePG_8$ to $LGePG_{10}$, K_{gl} is observed to increase. Though the K_{gl} of $LGePG_6$ is low compared to other samples of LGePG series, it has become our choice of interest because of two reasons: (a) low glass transition temperature (751 K) that would exhibit the good electrical properties, (b) optimum degree of crystallization by the precipitation of nanocrystallne phases which would yield correlation between the mean bond strength and cross-link density of the glassceramic networks. Hence, the transformation of amorphous phase (dis-order) into crystalline (order) expected to influence largely on the conduction features as a function of DTA parameters.

Our earlier investigation reported that Ga_2O_3 crystallites after 20 h of milling were precipitated with crystalline phases with optimum crystallization in glassceramic matrix (Reddy et al. 2012). XRD powder diffraction patterns were obtained on all the LGePG glassceramic samples at room temperature is to determine the phase compositions (Fig. 2). Broad crystalline peaks together with other broad and weak clusters of peaks centered at various 2θs in the patterns of all the samples attributed to the secondary phases with variable intensity. The nanocrystalline phases such as $LiGe_2(PO_4)_3$ (NASICON type) and, $Ga_2Li_3(PO_3)_7$ were identified from major diffraction peaks of LGePG samples (Reddy et al. 2015) and these phases were justified by the first and second exothermic peaks in DTA traces (Fig. 1). Nevertheless, there are some weak peaks corresponding to the GeO_2 phase and some very weak peaks which are yet to be identified. The NASICON-type phase of $LiGe_2(PO_4)_3$ is observed predominantly as depicted in Fig. 2, and its intensity increases with Ga_2O_3 content. Distances between XRD peaks of the samples and the horizontal axis were measured

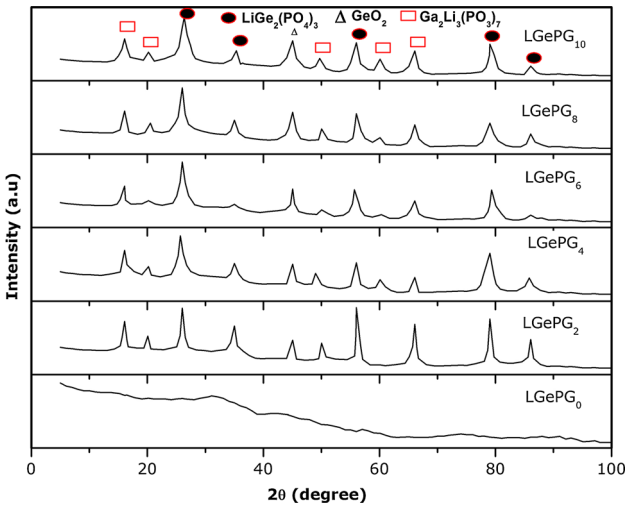

Fig. 2 XRD patterns of all the LGePG glassceramic samples

Table 2 Average percentages of crystallization at various 2θs for LGePG glassceramic samples

Sample	Avg. percentage crystallization
$LGePG_0$	–
$LGePG_2$	33.6
$LGePG_4$	43.5
$LGePG_6$	**58.9**
$LGePG_8$	67.2
$LGePG_{10}$	78.2

The best result is set in bold

at various 2θs (JCPDS File, Card no: 80-1922). The volume fraction of crystallization and relative to other for all the LGePG glassceramic samples was obtained by the Ohlberg and Strickler equation (Ohlbeg and Stricklet 1962). The average percentage of crystallization at various 2θs in all the LGePG glassceramic samples is shown in Table 2. The aluminum is absent in this type of phase and there is an every possibility for the partial substitution of ions having similar ionic radii such as Ge^{4+} by Al^{3+} during the transformation of glass into glassceramics which induces more Li^+ ions into the crystal structure, leading to boost the ionic conductivity in the present LGePG glass system. However, the massive crystallization in these glassceramic samples resulting to reduce the conducting features. One more conducting phase $Ga_2Li_3(PO_3)_7$ was also recorded in all the LGePG glassceramic samples which boosts up the electrical conductivity in addition with NASICON-type phase which appears as second exothermic peak in DTA trace (Fig. 1). On the other hand, the GeO_2 phase is identified as the most insulating phase, whose intensity is almost constant for all the samples of LGePG glassceramic system (Kim et al. 2006). As shown in Table 2, the secondary GeO_2 phase has

Table 3 Most important crystallographic parameters for crystalline phases for the highest conducting sample ($LGePG_6$)

Phase	Unit cell parameters			Quantitative volume fraction (%)
	a (Å)	*b* (Å)	*c* (Å)	
$LiGe_2(PO_4)_3$	8.2643	8.2645	2.5681	88.93
$Ga_2Li_3(PO_3)_7$	7.6503	7.6503	7.1230	8.49
GeO_2	5.0012	5.0012	5.5780	2.58

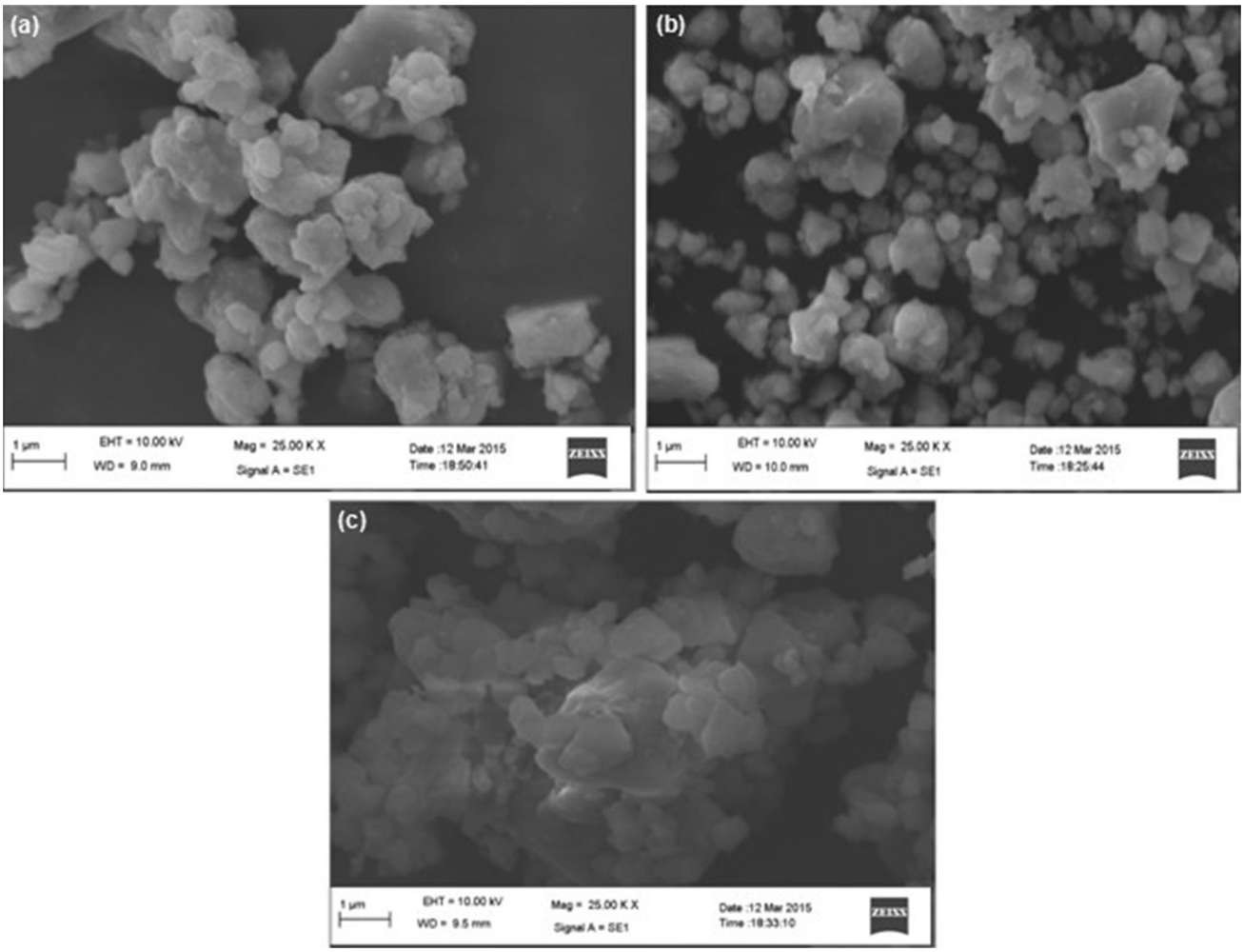

Fig. 3 SEM images of some **a** $LGePG_2$, **b** $LGePG_6$, **c** $LGePG_{10}$ glassceramic samples

appeared with small volume fraction (2.58 %) out of the average crystallization percentage of NASICON-type phase in $LGePG_6$ sample (Table 3) which does not affect much on the overall mechanism of crystallization of glass. The analysis reflects that the predominant NASICON-type phase ($LiGe_2(PO_4)_3$) which has been characterized as rhombohedral crystal system with a unit cell of dimensions $a = 8.2643$ Å, $b = 8.2645$ Å, $c = 2.5681$ Å and $\beta = 98.99°$, which is in agreement with the reported data (JCPDS card) and space group R3c. However, correlation between the quantitative volume fraction of crystalline phases (Table 3) and their electrical features of the LGePG glass-ceramic samples will be discussed in the next section.

SEM images of some samples are crucial to analyse crystallization behavior by considering the phase and microstructural details (Fig. 3). It can be seen from the Fig. 3, that crystalline phase appears with white region where as residual glass phase appears with black region. Figure 3a, c shows the presence of agglomerated grain like crystallites (170–300 nm) of major crystalline phases

[$LiGe_2(PO_4)_3$ (NASICON type), and $Ga_2Li_3(PO_3)_7$] precipitated along the grain boundaries. SEM image of $LGePG_6$ glassceramic sample (Fig. 3b) revealed the presence of interconnected fine and uniform grain crystallites (110–170 nm) of all the as mentioned major crystalline phases which are uniformly dispersed in the glass matrix and separated by well-developed grain boundaries throughout the micrograph. XRD pattern (Fig. 2) justified these grain-like crystallites belong to the major crystalline phases [$LiGe_2(PO_4)_3$ (NASICON type), and $Ga_2Li_3(PO_3)_7$]. Nevertheless, it can be seen from Fig. 3b that the crystal growth of crystallites is optimum and distributed by connective tissues of the $LGePG_6$ glassceramic matrix among all the samples under investigation. On the other hand, crystal growth of the crystallites is not perfect and uniform for rest of all other samples as synthesized. To get better conducting features via the presence of the ionically conductive, interfacial region between the glassy matrix and devitrified crystalline grain, further investigations require on the heat treatment schedule around the glass transition temperature (T_c) of these LGePG glassceramic samples.

The electrical properties of as synthesized glass and glassceramic samples were monitored using impedance spectroscopy (Kupracz et al. 2015). This technique is relatively powerful to investigate the dynamics of mobile charges in the bulk or interfacial regions of any kind of materials which operates an alternating current with variable frequency. The impedance data obtained were fitted to nonlinear least-square method. Here, the electrical properties can be associated to a parallel resistance and capacitance circuit corresponding to equivalent to the individual component of the materials (i.e., bulk and grain boundary) represents a semicircle and therefore bulk response of the sample is detected. Hence, the bulk conductivity may be evaluated for all the LGePG glassceramic samples from the impedance spectrum using the relation

$$\sigma_b = t/(R \cdot A) \quad (1)$$

where R is the bulk resistance which was determined from the intersection of the semicircle with the real axis of the impedance Z'; t the thickness, and A the surface area of the sample and is achieved to be highest for $LGePG_6$ sample ($\sigma = 8.31 \times 10^{-04}$ S/cm) at 303 K (Fig. 4). Compositional dependence of glass stability parameter (K_{gl}) and bulk conductivity (σ_b) for all the LGePG glassceramic samples are depicted in Fig. 4. The lowest value of glass stability parameter (K_{gl}) for the highest conducting $LGePG_6$ sample indicates that optimum degree of its crystallization achieved by the precipitation of nanocrystalline phases boosting the conductivity features as justified by XRD patterns and SEM images (Milankovic et al. 1997; Garbarczyk et al. 2006).

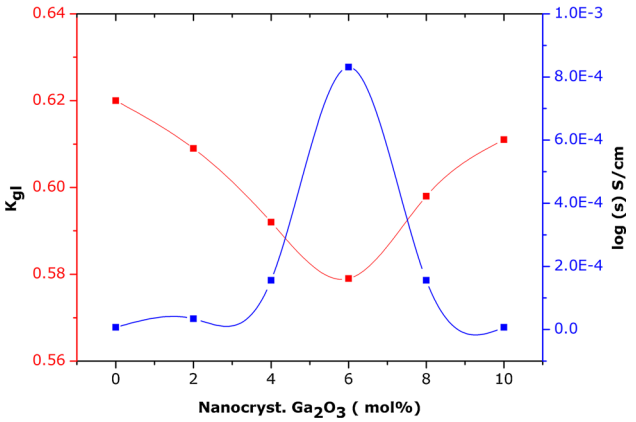

Fig. 4 Variation of glass forming ability parameter (K_{gl}) and log(σ) (at 303 K) with nanocrystal Ga_2O_3 (mol%) for all the LGePG samples

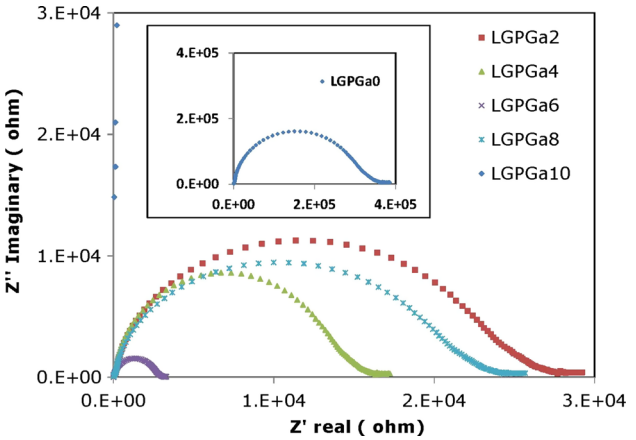

Fig. 5 Complex impedance spectra (Z'' vs Z') for all the LGePG glassceramic samples at 303 K

The Nyquist plots between (Z'' vs Z') for all the LGePG glassceramic samples measured at 303 K and for highest conducting sample $LGePG_6$ at different temperatures are shown in Figs. 5 and 6. The impedance spectrum was found to exhibit single semicircular arc which shows that the electrical properties of present samples arises due to bulk effects. Bulk conductivity of all the glassceramic samples at different temperatures (303–423 K) is obtained by using the resistance (R) obtained from the analyzed impedance data and pellet dimensions. It can be seen that increase in temperature caused the impedance semicircles to be shifted to lower and lower Z' values which indicates the decrease in the resistive property of the material (Fig. 6).

The conductivity data are fitted to the Arrhenius equation

$$\sigma_{dc} = \sigma_0 \exp(-E_{a\sigma}/kT) \quad (2)$$

σ_0 is the pre exponential factor and $E_{a\sigma}$, k and T are the activation energy for the conduction, Boltzman's constant

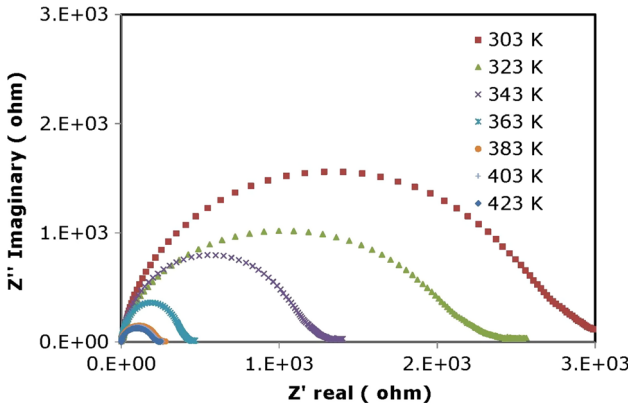

Fig. 6 Impedance spectra (Z'' vs Z') for the highest conducting sample $LGePG_6$ at different temperatures (303–423 K)

(1.3806×10^{-22} J/K) and absolute temperature, respectively. The activation energy for conduction ($E_{a\sigma}$) was calculated from the slope of the straight lines obtained when the data is plotted against $1000/T$ of all the glassceramic samples. The slope is calculated as follows. ($-E_{a\sigma}/kT$) is the slope and Eq. (2) can be written as

$$\ln(\sigma) = \ln(A)\text{slope}\left(\frac{1}{T}\right) \tag{3}$$

and the value of slope can be calculated from the linear graph of $\ln(\sigma)$ vs $\frac{1}{T}$ as follows

$$\text{Slope} = \frac{\Delta \ln(\sigma)}{\Delta \frac{1}{T}} \tag{4}$$

The activation energy for conduction ($E_{a\sigma}$) is now calculated as $E_{a\sigma} = -k \times$ slope. The slope being negative, a positive value of $E_{a\sigma}$ is obtained.

The compositional dependence of activation energy for conduction ($E_{a\sigma}$) for all the LGePG glassceramic samples at 303 K is shown in the Fig. 7. It is observed that the activation energy is found to be the lowest for the highest conducting sample $LGePG_6$ (Fig. 7) and it does not show the nonlinear behavior of conductivity which reveals that the variation of mobile Li^+ ion conductivity is directly related to the percentage of crystallization (Panmand et al. 2010; Raghavan and Rao 1996; Xiaoxiong et al. 2006). The same has been justified by the intensity and broadening of XRD peaks of $LGePG_6$ among all the samples under investigation with optimum crystallization (58.9 %). Hence, the increased mobility of Li^+ ions in addition to the percentage of crystallization plays a vital role in boosting the conductivity of the LGePG series of samples (Heitjansa et al. 2008; Garbarczyk et al. 2006).

The frequency-dependent electrical conductivity fulfills the power-law equation

$$\sigma_{\text{ac}} = \sigma_o + A\omega^s \tag{5}$$

where characteristic parameter 's' lies in between zero and one and decreases slightly with increasing temperature. In general, the low-frequency part of the conductivity is frequency independent and the frequency-independent conductivity (σ_o) is obtained by extrapolation of the conductivity approaches to the frequency as zero. Conductivity exhibits the dispersion at the high-frequency region and increases in a power-law fashion (Nobre and Lafendri 2001). AC conductivity plots as a function of frequency for all the LGePG samples at 303 K are shown in Fig. 8. It is to be noted down that change in the slope of ac conductivity with frequency concludes domination of grain resistance over grain boundary resistance for a particular temperature (Sambasiva Rao et al. 2008). The small deviation from σ_{dc} in the frequency-independent part of the conductivity reflects the influence of electrode polarization in the glassceramic samples. Critical frequency is frequency ($\omega_p = f_o$), at which the conductivity deviates from the frequency-independent part. The shift in the critical frequency towards higher frequency side on increasing

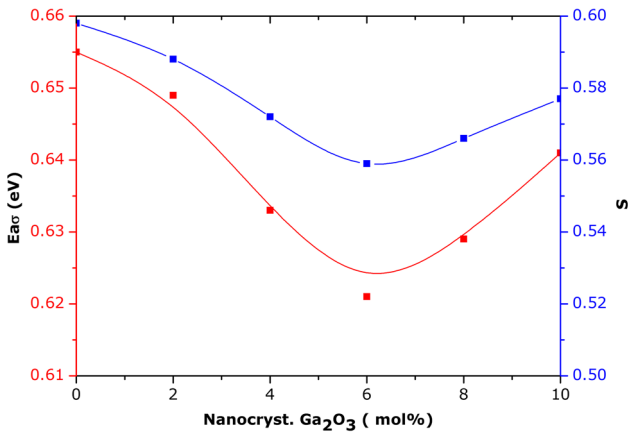

Fig. 7 Compositional dependence of activation energy for conduction ($E_{a\sigma}$) and characteristic parameter (s) measured at 303 K

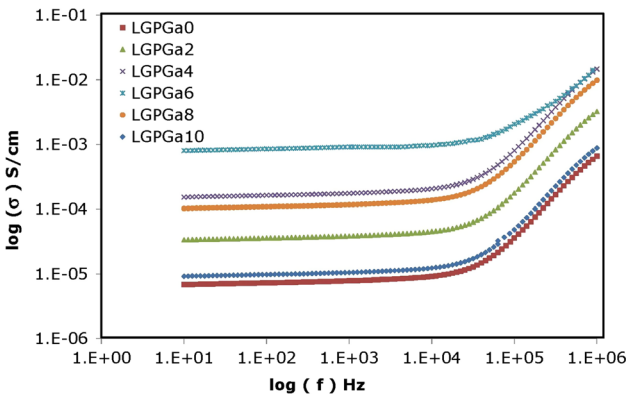

Fig. 8 Log(σ) versus log(f) plots for all the LGePG glassceramic samples measured at 303 K

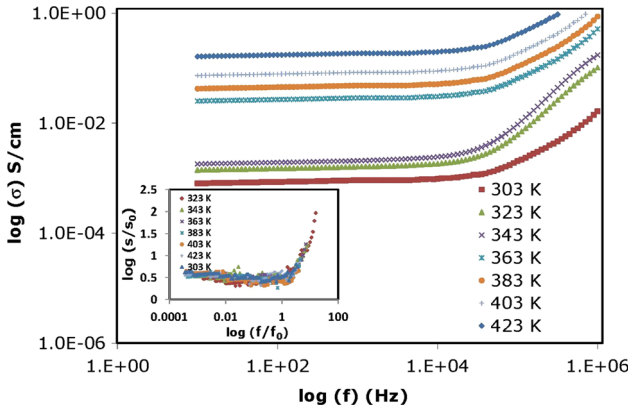

Fig. 9 Log(σ) versus log(f) plots for highest conducting sample $LGePG_6$ at different temperatures (303–423 K). *Inset* shows normalized plots of electrical conductivity for highest conducting sample $LGePG_6$ at different temperatures (303–423 K)

temperature is a little more obvious for the ac conductivity of $LGePG_6$ at different temperatures (Fig. 9). Nevertheless, the relation between frequency-independent conductivity σ_0 and the critical frequency (f_o) can be represented by the following equation:

$$\sigma_o = Kf_o, \tag{6}$$

where $K = (Ne^2a^2/kT)vc(1-c)$, is the empirical constant that depends on the concentration of mobile ions, temperature and the conduction mechanism (Jain et al. 1993). In the equation for K, v is the geometrical factor which includes the correlated factor, c is the concentration of mobile ions on N equivalent lattices per unit volume, a is the hopping distance, e is the electronic charge, T is absolute temperature and k is Boltzman's constant. The relaxation effects begin to appear at the critical frequency (f_o), which moves towards the higher frequency with an increase in the temperature of the measurement. Further, it is observed that the critical frequency (f_o) is thermally activated with the same activation energy as that of the conductivity $\sigma_0 T$ (Verhoef and den Hartog 1994).

Compositional dependence of characteristic parameter (s) is known to be material dependent and its value is observed to be the lowest for highest conducting sample $LGePG_6$ (Fig. 7). A summary of the electrical conductivity, activation energy and characteristic parameters is given in Table 4. The frequency-independent part and dependent parts of the conductivity may be explained by long-range transport of Li^+ ions and diffusion controlled relaxation model (Elliot and Owens 1994).

To explore the further information about the dependence of the ion transport on the composition, temperature, structure, and also on the concentration of the charge carriers, the ac conductivity data obtained at various temperatures for $LGePG_6$ at different temperatures have been scaled and are presented in the inset of Fig. 9 (Karmakar et al. 2009). Perfect overlapping of normalized imaginary part of AC conductivity plots of LGePG samples suggested the conduction transport mechanism to be temperature independent. The contribution of highly conductive phases such as NASICON-type phase of $LiGe_2(PO_4)_3$ in addition with another conducting phase $Ga_2Li_3(PO_3)_7$ is boosting the ac conductivity from $LGePG_0$ to $LGePG_6$ (Kun et al. 2011). On the other hand, the highest conductivity is achieved to be ($\sigma = 8.31 \times 10^{-04}$ S/cm) for $LGePG_6$ sample which is expected due to the optimum percentage of crystallization 58.9 % (Table 2) and the presence of uniform distribution of conducting crystalline phases. However, the massive crystallization results to decrease the conductivity from $LGePG_8$ to $LGePG_{10}$ (Garbarczyk et al. 2006). In this process, we have monitored variation of imaginary permittivity (ε'') with frequency, where the imaginary part ε'' is exceeded by the dc conductivity and will not be discussed further and hence, the modulus formalism was used for the further analysis.

Electrical modulus formulation is a convenient tool to explore electrical transport phenomenon of the material. Also, it pacifies the noise of extrinsic relaxation often used in the analysis of electrode polarization and bulk phenomena such as average conductivity relaxation times τ_σ of ionically conducting glasses (Mc Crum et al. 1967; Moynihan 1994; Moynihan et al. 1973).

It is speculated that the simultaneous application of both impedance (Z'' vs Z') and modulus (M'' vs M') spectroscopy

Table 4 Summary of conductivity (σ), activation energy ($E_{a\sigma}$ and $E_{a\tau}$) characteristic parameter (s) and stretched exponent (β) and relaxation time (τ) of LGePG glassceramic samples

Glass	σ (303 K) S/cm	$E_{a\sigma}$ (eV)	s (303 K)	$E_{a\tau}$ (eV)	β (303 K)	τ (10^{-6} s) 303 K
$LGePG_0$	(6.96 ± 0.81)E−06	0.655 ± 0.007	0.598	0.648 ± 0.005	0.551	2.52
$LGePG_2$	(3.43 ± 0.74)E−05	0.649 ± 0.005	0.588	0.64 ± 0.006	0.539	2.21
$LGePG_4$	(1.56 ± 0.89)E−04	0.633 ± 0.006	0.572	0.632 ± 0.004	0.522	1.78
$LGePG_6$	**(8.31 ± 0.79)E−04**	**0.621 ± 0.008**	**0.559**	**0.618 ± 0.001**	**0.518**	**1.57**
$LGePG_8$	(1.56 ± 0.91)E−04	0.629 ± 0.003	0.566	0.622 ± 0.006	0.529	1.42
$LGePG_{10}$	(6.96 ± 0.93)E−06	0.641 ± 0.007	0.577	0.644 ± 0.003	0.534	1.26

The best result is set in bold

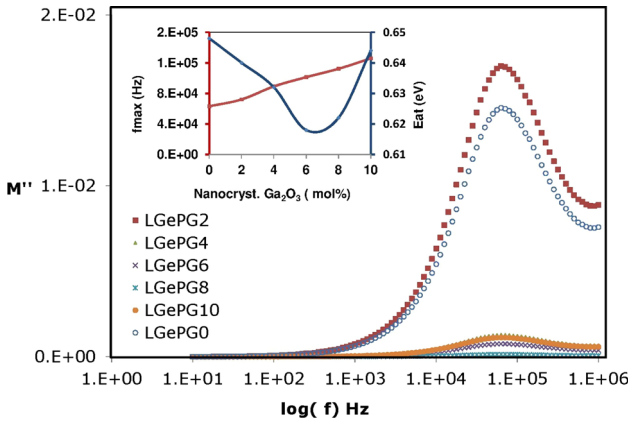

Fig. 10 Electric modulus (M'') versus log(f) plots for all the LGePG glassceramic samples measured at 303 K. *Inset* shows the compositional dependence of variation of activation energy for relaxation ($E_{a\tau}$) and f_{max} measured at 303 K

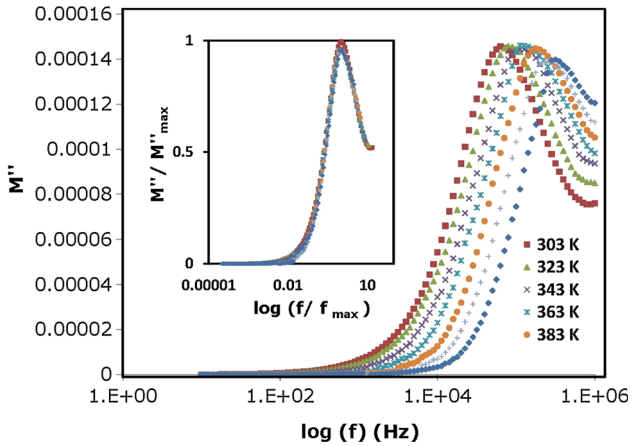

Fig. 11 Electric modulus (M'') versus log(f) plots the highest conducting glass ceramic sample $LGePG_6$ measured at at different temperatures (303–423 K). Normalized plots of electric modulus of the highest conducting sample ($LGePG_6$) at different temperatures 303–423 K

would deal to rationalize the dielectric properties (Sinclair and West 1989, 1997). In view of technological importance, we have analysed both electrical conductivity and modulus formalisms simultaneously, in this investigation. Figures 10 and 11 show the frequency dependence of imaginary part of electric modulus M'' for all the LGePG samples at 303 K and for highest conducting sample $LGePG_6$ at different temperatures (303–423 K). The M'' value is observed to be constant (M''_{max}) at a relaxation frequency (f_{max}) and the peak M''_{max} symmetrically shifts towards higher frequencies with increasing temperatures (Fig. 11). This behavior suggests that the dielectric relaxation is not the usual thermally activated type in which hopping mechanism of charge carriers dominates

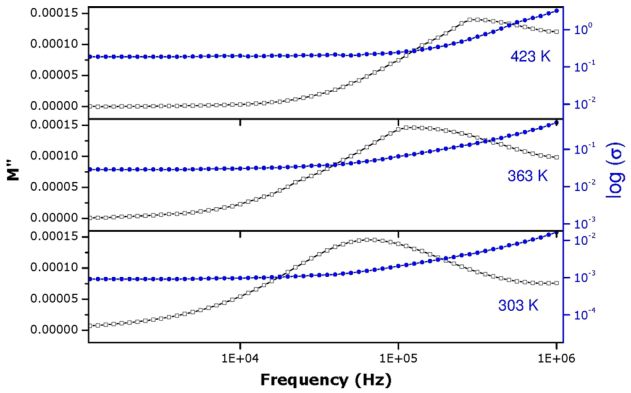

Fig. 12 Frequency (log f) vs bulk conductivity (log σ) and imaginary part of electric modulus (M'') at three different temperatures (323, 363 and 423 K) of $LGePG_6$

intrinsically. From Fig. 10, the relaxation frequency (f_{max}) corresponding to the maximum in M'' curves and the relaxation time τ, calculated using the relation $\tau = 1/2\pi f_{max}$ at different temperatures can be obtained and presented in Table 4. Nevertheless, the activation energy for the conductivity relaxation $E_{a\tau}$ for all the LGePG samples was calculated from the relaxation time plots and the values of $E_{a\tau}$ and $E_{a\sigma}$ are in good agreement with each other (Table 4) which suggest that the ionic-hopping mechanism responsible for the relaxation is the same as that for the conductivity (Chowdari et al. 1990). In principle, full width half maximum (β) can be calculated by the width at the half maxima for any bell shaped curve and the same method was adopted for all the frequency-dependent electrical modulus curves (Fig. 10). The full width half maximum (β) and characteristic relaxation time (τ) of M'' peaks are given in Table 4. The value of β is lowest for the highest conducting sample $LGePG_6$, which justifies its optimum percentage of crystallization as supported in the XRD analysis leading to modify the conductivity in the neighborhood of conduction path. The overlap of critical frequency (f_o) of log(σ) peaks and relaxation frequency of and M'' peaks for the highest conducting sample $LGePG_6$ at different temperatures (323, 363 and 423 K) have been demonstrated to be a result from the same mechanism and this result is further confirmed that the two processes are closely correlated with each other (Fig. 12). As the temperature increases, the same corresponding peak shifts to a higher frequency but they present the same characteristic relaxation time at specific temperatures. Nevertheless, the peak in log(σ) is slightly shifted to a higher frequency with respect to the M'' peak position in all LGePG samples which suggests the presence of possibly more than one mechanism but this contribution does not influence the overall conductivity response that much as it was determined that the activation energies calculated from the conductivity curves and those of the relaxation were

essentially the same. This is supported by master curves in the normalized plots of electric modulus spectra (inset of Fig. 11), which suggests that the dynamical relaxation processes in the LGePG samples is temperature independent. The β values show that the conductivity relaxation is to be highly nonexponential with increasing temperature (Table 4).

Conclusions

The lowest value of K_{gl} for the glassceramic sample $LGePG_6$ (0.517), denotes the decrease in the degree of de-polymerization which possesses fast diffusion pathways, leading to achieve good compatibility between electrodes. XRD patterns pointed out that the $LGePG_6$ sample exhibits the optimum crystallization of nanocrystalline phases such as $LiGe_2(PO_4)_3$ (NASICON type), $Ga_2Li_3(PO_3)_7$ from major diffraction peaks. SEM pictures revealed that $LGePG_6$ glassceramic sample is observed to be interconnected fine and uniform crystallites of major crystalline phases ($LiGe_2(PO_4)_3$ (NASICON type), $Ga_2Li_3(PO_3)7$) which are uniformly dispersed in the glass matrix and separated by well-developed grain boundaries which is justified by XRD pattern. The bulk conductivity is achieved to be the highest for $LGePG_6$ sample (8.31×10^{-04} S/cm). The M'' spectra shows non-Debye type relaxation and shift to higher frequency side for the sample $LGePG_6$ with the highest conductivity due to the increase of mobile charge carriers and the same would be applicable for all the other samples under investigation. The modulus scaling spectra show that the dynamical relaxation processes is temperature independent for a particular composition. The β exponent value indicates that the conductivity relaxation is highly nonexponential (Table 4).

References

Al-Hartomy OA, Al-Ghamdi AA, El-Tantawy F, El-Desoky MM (2013) Effect of nanocrystallization on the structural and electrical conductivity enhancement of vanadium-based glasses. J Mater Sci 48:3067–3074

Chowdari BVR, Krishnan RG, Ghosh SH, Tan KL (1990) Thermal, electrical and structural characterization of $Li_2O{\cdot}P_2O_5{\cdot}MoO_3$ glasses. Solid State Ionics 40–41(2):684–688

Dell LAO, Savin SLO, Chadwick AV, Smith ME (2007) Multi nuclear MAS NMR investigation of sol–gel and ball milled nanocrystalline Ga_2O_3. Appl Mag Reson 32:527–546

El-Desoky MM (2010) Gaint electrical conductivity enhancement in BaO-V_2O_5-Bi_2O_3 glass by nanocrystallization. Mater Chem Phys 119:389–394

Elliot SR, Owens AP (1994) Frequency-dependent conductivity in ionically and electronically conducting amorphous solids. Solid State Ionics 70:27

Fanelli E, Pernice P, Xiao M, Sigaev VN (2011) Crystallization behaviour and nanostructuring in alkali niobiosilicate glasses. J Mater Sci Technol 27(2):189–192

Garbarczyk JE, Jozwiak P, Wasiucionek M, Nowinski JL (2006) Effect of nanocrystallization on the electronic conductivity of vanadate–phosphate glasses. Solid State Ionics 177:2585–2588

Hayashi A, Noi K, Sakuda A, Tatsumisago M (2012) Superionic glassceramic electrolytes for room-temperature rechargeable sodium batteries. Nat Commun 3:856–860

He K, Zu C, Wang Y, Han B, Yin X, Zhao H (2014) Stability of lithium ion conductor NASICON structure glass ceramic in acid and alkaline aqueous solution. Solid State Ionics 254:78–81

Heitjansa P, Tobschallb E, Wilkening M (2008) Ion transport and diffusion in nanocrystalline and glassy ceramics Eur. Phys J Spec Topics 161:97

Hruby A (1972) Evalution of glass-forming tendency by means of DTA. Czech J Phys B 22(11):1187–1193

Jain H, Kanert O (1993) In: Spaeth JM (eds) Proceedings of the XII international conference on defects in insulting materials, vol 1. World Scientific Co, p 274

Kang D, Han M, Lee SG (2003) Dielectric and pyroelectric properties of barium strontium calcium titanate ceramics. J Eur Cerm Soc 23(3):515–518

Karmakar A, Majumdar S, Giri S (2009) Polaron relaxation and hopping conductivity in $LaMn_{1-x}Fe_xO_3$. Phys Rev B 79:094406/1–094406/7

Kim H-S, Jeong C-S (2011) Electrochemical properties of binary electrolytes for lithium-sulfur batteries. Bull Korean Chem Soc 32:3682–3686

Kim Y, Saienga J, Martin SW (2006) Anomalous ionic conductivity increase in Li_2S–GeS_2–GeO_2 glasses. J Phys Chem B 110(33):16318–16325

Kim Y, Hwang H, Lawler K, Martin SW, Cho J (2008) Electrochemical behavior of Ge and GeX_2 (X = O, S) glasses: improved reversibility of the reaction of Li with Ge in a sulfide medium. Electrochim Acta 53:5058–5064

Kun HE, Yan-Hang W, Cheng-Kui Z, Yong-Hua L, Hui Feng Z, Bin H, Jiang C (2011) Microstrucutre and Ionic conductivity of Li_2O–Al_2O_3–GeO_2–P_2O_5 glassceramics. Chin J Inorg Chem 27(12):2484–2488

Kupracz P, Karczewski J, Prześniak-Welenc M, Szreder NA, Winiarski MJ, Klimczuk T, Barczy'nski RJ (2015) Micrsostructure and electrical properties of manganese borosilicate glasses. Non-Cryst Solids 423–424:68–75

Lam HM, Hong MH, Yuan S, Chong C (2004) Growth of β-Ga_2O_3 nanoparticles by pulsed laser ablation technique. Appl Phys A 79(8):2099–2102

$LiGe_2$ $(PO_4)_3$—JCPDS powder diffraction file, card no. 80-1922. Joint Committee on Powder diffraction Standards (JCPDS), Swarthmore

Mc Crum NG, Read BE, Williams G (1967) Anelastic and dielectric effects in polymeric solids. Wiley, New York

Milankovic AM, Furic K, Day DE (1997) Raman studies of PbO–Bi_2O_3–Ga_2O_3 glasses and crystallized compositions. Phys Chem Glasses 38:148–150

Moynihan CT (1994) Analysis of electrical relaxation in glasses and melts with large concentrations of mobile ions. J Non-Cryst Solids 172–174:1395–1407

Moynihan CT, Boesch LP, Laberge NL (1973) Decay function for the electric field relaxation in vitreous ionic conductors. Phys Chem Glasses 14:122–125

Nobre MAL, Lafendri S (2001) Phase transition in sodium lithium niobate polycrystal: an overview based on impedance spectroscopy. J Phys Chem Solids 21:999

Ohlbeg SM, Stricklet DW (1962) Effects of composition changes on the crystallization behavior and properties of SiO_2–Al_2O_3–CaO–MgO (Fe_2O_3–Na_2O–K_2O). J Am Ceram Soc 45:170–172

Panmand RP, Kawade UV, Kulkarni MV, Apte SK, Kale BB, Gosavi SW (2010) Synthesis and characterization of Bi_2S_3 nanosrystals in glass matrix. Mater Sci Eng B 168:161

Prasad SVGVA, Bhaskaran GS, Veeraiah N (2005) Spectroscopic, magnetic and dielectric investigations of BaO–Ga_2O_3–P_2O_5 glasses doped by Cu ions. Phys Sta Soli A 202:2812–2828

Raghavan MS, Rao KJSL (1996) Electrical transport studies in alkali borovanadate glasses. J Phys Chem 100:4243

Reddy CKK, Balaji Rao R, Koti Reddy CV (2012) Influence of nanocrystalline phases on the electrical properties of lithium titanate phosphate glassceramics mixed with Ga_2O_3 nanocrystals. J Phase Transit 85:218

Reddy CKK, Balaji Rao R, Gopal Reddy C (2015) The role of crystallization on microstructural and electrical studies of lithium germanium phosphate glass-ceramic electrolytes. Ionics 21:967–979

Sambasiva Rao K, Murali Krishna P, Swarna Latha T, Madhava Prasad D (2008) Impedance spectroscopy analysis and piezoelectric properties of Pb2KNb5O5 ceramics. Mater Sci Eng B 131(1):127

Sinclair DC, West AR (1989) Impedance and modulus spectroscopy of $BaTiO_3$ showing positive temperature coefficient of resistance. J Appl Phys 66:3850–3856

Sinclair DC, West AR (1997) Characterization of electrical materials, especially ferroelectrics, by impedance spectroscopy. J Electroceram 1(1):65–71

Verhoef AH, den Hartog HW (1994) High frequency dielectric properties of alkali and alkali-halide borate glasses. Solid State Ionics 68:305

Xiaoxiong XU, Zhaoyin W, Xuelin Y, Gu Z (2006) Ionic conductivity and microstructural evaluton of Li_2O–TiO_2–P_2O_5–SiO_2 glass ceramics. Solid State Ionics 177:2611

Xu H, Gao L (2004) Hydrothermal synthesis of high purity $BaTiO_3$ powders: control of powder phase and size, sintering density and dielectric properties. Mater Lett 58:1582–1586